

# Local and average crystal structure and displacements of $\text{La}^{11}\text{B}_6$ and $\text{EuB}_6$ as a function of temperature

C. H. Booth,<sup>1,2,†</sup> J. L. Sarrao,<sup>2</sup> M. F. Hundley,<sup>2</sup> A. L. Cornelius,<sup>2,3</sup>  
G. H. Kwei,<sup>2</sup> A. Bianchi,<sup>4</sup> Z. Fisk,<sup>4</sup> and J. M. Lawrence<sup>5</sup>

<sup>1</sup>*Chemical Sciences Division, Lawrence Berkeley National Laboratory, Berkeley, California 94720*

<sup>2</sup>*Los Alamos National Laboratory, Los Alamos, New Mexico 87545*

<sup>3</sup>*Department of Physics, University of Nevada-Las Vegas,*

*4505 Maryland Parkway, Box 454002, Las Vegas, Nevada 89154-4002*

<sup>4</sup>*Department of Physics and National High Magnetic Field Laboratory Florida State University, Tallahassee, Florida 32306*

<sup>5</sup>*Physics Department, University of California, Irvine, California 92697*

(Dated: submitted to Phys. Rev. B)

Measurements of both the average crystal structure from Rietveld refinement of neutron powder diffraction (NPD) data and the local structure from La  $L_{\text{III}}$ -edge x-ray-absorption fine-structure (XAFS) are presented for a  $\text{La}^{11}\text{B}_6$  sample as a function of temperature ( $\sim 10$ -320 K). These data are compared to XAFS results on a  $\text{EuB}_6$  sample. The single-site La and B positional distribution widths and the La-B and La-La bond length distribution widths and their temperature dependence are compared. This comparison allows an estimate of the La and B site displacements, and we find that these sublattices are only slightly correlated with each other. Moreover, while the temperature dependence of the displacement parameters of the average sites from diffraction fit an Einstein model well, the temperature dependence of the La-B bond length distribution width requires at least two vibrational frequencies, corresponding to the La and B frequencies of the individual sites. XAFS data on  $\text{EuB}_6$  indicate that the situation is the same in the Eu compound. In addition, comparisons between data taken below and above the ferromagnetic transition temperature for  $\text{EuB}_6$  place stringent limits on the lattice involvement in the associated metal-insulator transition and the ensuing large magnetoresistance effect. This lack of lattice involvement in the magnetoresistance transition is in sharp contrast to the strong lattice involvement observed in the colossal magnetoresistance lanthanum manganese perovskites.

PACS numbers: 71.38.-k 71.30.+h 61.10.Ht 61.12.Ld

## I. INTRODUCTION

The  $\text{AB}_6$  hexaborides possess a wide range of interesting electronic and magnetic properties, including mixed valence, heavy fermion, metallic, superconducting and semiconducting behavior.<sup>1</sup>  $\text{EuB}_6$  is perhaps the least understood hexaboride. To begin with, although all the hexaborides share the same crystal structure (Fig. 1), Eu is one of the few metals in the hexaboride series that is divalent rather than trivalent (Sr, Ca and Yb are the others). The divalent hexaborides are believed<sup>2</sup> to be semimetals, and  $\text{EuB}_6$  is consistent with this expectation.<sup>3,4</sup> Above room temperature it appears to behave as a semiconductor, but as the temperature is lowered below room temperature, the resistivity (Fig. 2) decreases, as in a metal.<sup>5</sup> As the temperature is lowered to about 16 K, the resistivity then increases, followed by a precipitous drop. This “metal insulator” transition at 15.5 K is concomitant with a partial ( $\sim 15\%$ ) ferromagnetic alignment of the Eu spins.<sup>5</sup> The resistivity and specific heat also exhibit a second (albeit broad) transition at about 12.6 K (inset of Fig. 2) at which the majority of Eu spins become ferromagnetically aligned. In addition,

there is a large negative magnetoresistance (MR) effect of about 95% in 5 T at temperatures near  $T_C$ .

Although the magnitude and overall character of this MR effect is different in detail than the colossal magnetoresistance (CMR) lanthanum manganese perovskites,<sup>6</sup> the presence of a MI transition in the vicinity of a FM transition and a large MR effect has prompted comparisons to the perovskites as a possible place to look for clues about the nature of the behavior of  $\text{EuB}_6$ .<sup>7</sup> One important point is that just above the transition, the resistance shows a sharp increase with decreasing temperature (Fig. 2), consistent with a short temperature range where activated behavior could exist, as expected for polaron transport. In fact, short-range magnetic order (i.e. magnetic polarons) at temperatures above  $T_C$  have been observed by Raman scattering.<sup>8</sup> A strong relationship between the magnetic polarons and transport properties has been conjectured.<sup>5</sup> Although the existence of magnetic polarons does not require associated lattice distortions (lattice polarons), some evidence suggests that the role of the lattice is still not understood. For instance, an unusually low-lying optical mode at  $145\text{ cm}^{-1}$  corresponding to relative motion between Eu and B atoms has

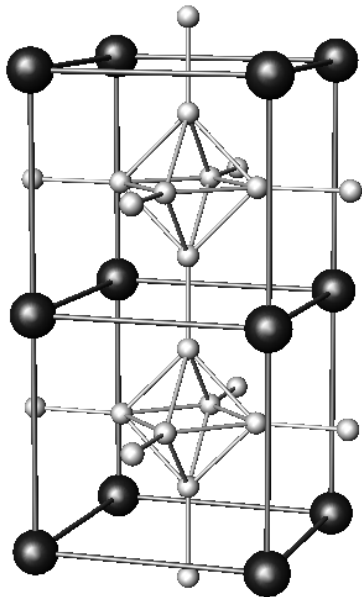


FIG. 1: Hexaboride crystal structure. Dark atoms represent a rare-earth and the light atoms represent boron. Two unit cells are shown to emphasize the shortest bond length in the structure, namely, the B-B pair between adjacent  $B_6$  octahedra.

been observed.<sup>7</sup> Moreover, group theory indicates that no ferromagnetic phases should exist within the measured  $Pm3m$  lattice symmetry.<sup>9</sup> Therefore, the actual symmetry of the  $EuB_6$  lattice must be lower, and indeed, some anisotropy in certain lattice reflections has been observed.<sup>10</sup>

Note that significant differences between  $EuB_6$  and the CMR perovskites have been observed. For instance, the analysis of the Raman scattering suggests that the number of Eu atoms that participate in the magnetic polarons is small ( $\sim 3\%$ ) compared to the perovskites ( $\gtrsim 20\%$ ). Furthermore, most of the hexaborides are crystallographically very well ordered ( $LaB_6$  is, in fact, often used as an x-ray diffraction standard because of its narrow diffraction peaks), and no change in the  $EuB_6$  lattice constant occurs near  $T_C$  to within  $0.0005 \text{ \AA}$ . However, pathological disorder can exist that is more easily observed with a local probe (the perovskites are a good example<sup>11</sup>), and given the evidence for magnetic polarons and the surprising paucity of temperature-dependent Rietveld refinements of  $LaB_6$  and  $EuB_6$ , a temperature-dependent local and average structural study is still necessary. Therefore, we performed both x-ray absorption fine-structure (XAFS) and neutron powder diffraction (NPD) experiments to elucidate the average and local structures of  $LaB_6$  and  $EuB_6$  and the relationship between them.

## II. EXPERIMENTAL DETAILS

Hexaboride samples were prepared by slow cooling dilute, stoichiometric amounts of the rare earth (La or Eu) and boron in aluminum, from  $1500 \text{ }^\circ\text{C}$ . Crystals were produced by leaching the aluminum in a NaOH solution. A large quantity ( $\approx 40 \text{ g}$ ) of  $La^{11}B_6$  was required for the NPD experiment in anticipation of using this same data for a pair-distribution function analysis in the future. Therefore, several batches were grown and mixed together and ground gently to form the final sample used for NPD. A small amount of one of these batches ( $\approx 10 \text{ mg}$ ) was used for the XAFS experiments. Both the polycrystalline  $La^{11}B_6$  and the single crystal of  $EuB_6$  used in the XAFS experiments were ground into a fine powder, passed through a  $30 \text{ }\mu\text{m}$  sieve, and brushed onto tape. Strips of tape were stacked such that the absorption step at the rare-earth  $L_{III}$  edge corresponded to about one absorption length.

Neutron powder diffraction data were collected on the General Purpose Powder Diffractometer (GPPD) instrument at the Intense Pulsed Neutron Source (IPNS) at Argonne National Laboratory with sample temperatures between  $10\text{-}300 \text{ K}$ . Since naturally occurring boron is a strong neutron absorber, we used  $LaB_6$  samples with  $>98\%$   $^{11}B$ .  $EuB_6$  was not measured in this manner since all Eu isotopes are also strong neutron absorbers. The structure was Rietveld refined using the GSAS software package.<sup>12</sup> The first four banks from GPPD corresponding to  $\pm 90^\circ$  and  $\pm 145^\circ$  were used in the refinement. The background scattering for each bank was modeled with a 5<sup>th</sup>-order polynomial in  $Q^2$ . Diffractometer constants were calibrated by fitting a room temperature scan of nickel powder. Even with a  $^{11}B$ -enriched sample, a large absorption coefficient was necessary to fit the hexaboride data, and because of a large correlation with the extinction parameter, we had to hold extinction equal to zero for these fits.

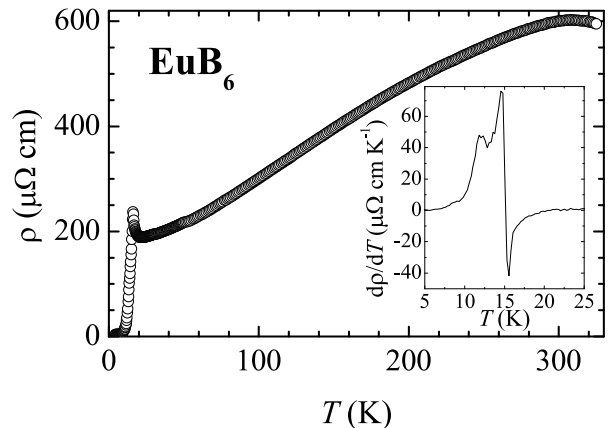


FIG. 2: Resistivity  $\rho$  of  $EuB_6$ . Inset shows  $\partial\rho/\partial T$  in the vicinity of the ferromagnetic transition.

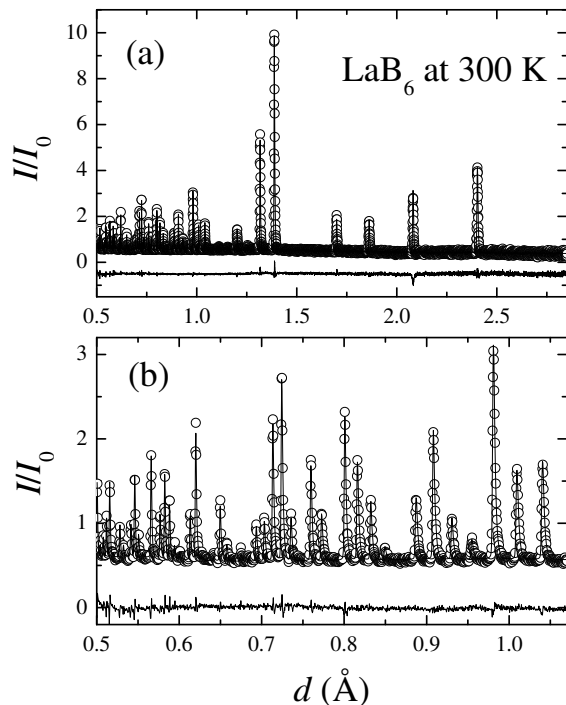


FIG. 3: Neutron powder diffraction data at 300 K on  $\text{LaB}_6$ , together with the fit and residual. Panel (b) expands the low- $d$  part of panel (a).

X-ray absorption fine-structure data were collected on BL 2-3 and 4-1 at the Stanford Synchrotron Radiation Laboratory (SSRL) from the La and Eu  $L_{\text{III}}$  edges for both  $\text{LaB}_6$  and  $\text{EuB}_6$  samples. The data range is limited in each case by the proximity of the  $L_{\text{II}}$  edge. A LHe-flow cryostat was used for data collected between 3.3 K and 300 K. Data above room temperature utilized an oven with the sample in a flowing He gas. A Si(111) double-crystal monochromator was used to collect  $\text{LaB}_6$  data, detuned by  $\approx 50\%$  to remove higher harmonics. A similar Si(220) crystal was used for the  $\text{EuB}_6$  data.

The XAFS data were reduced and fit in  $r$ -space using standard procedures.<sup>13,14</sup> In particular, absorption from other excitations (pre-edge absorption) was removed by fitting the data to a Victoreen formula, and a cubic spline (5 knots) was used to simulate the embedded-atom absorption  $\mu_0$ . The XAFS oscillations  $\chi$  were then obtained as a function of photoelectron wave vector  $k = \sqrt{2m_e(E - E_0)/\hbar^2}$  from  $\chi(k) = \mu/\mu_0 - 1$ .  $E_0$  of the samples was determined from the half-height of the main edge. Fits to the data were performed in  $r$ -space after Fourier transforming (FT)  $k\chi(k)$ . The real and imaginary parts of this transform are complicated functions of the scattering potentials, including a shift in the Fourier-transform peak positions from the actual bond lengths. We fit with backscattering amplitudes and phases calculated by the FEFF7 code,<sup>15</sup> which has been shown to

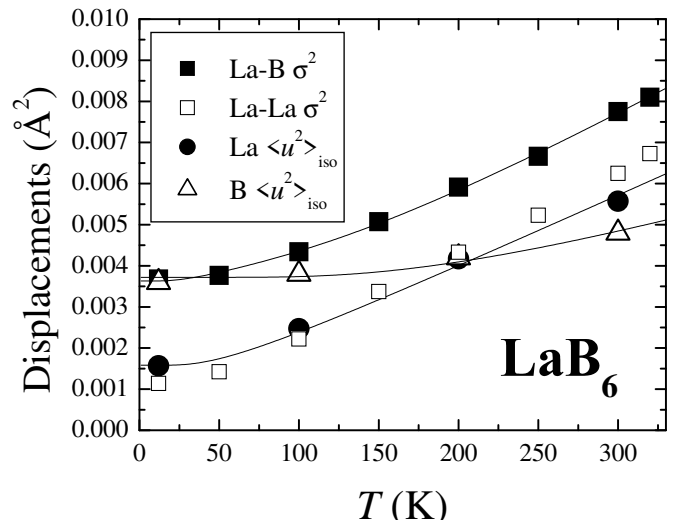


FIG. 4: Mean-squared displacements for the individual sites and near-neighbor pairs in  $\text{La}^{11}\text{B}_6$  as measured by NPD and XAFS, respectively. The anisotropic mean-squared displacements for boron are spherically averaged:  $\langle u_{\text{iso}}^2 \rangle = \frac{1}{3}(\langle u_{11}^2 \rangle + \langle u_{22}^2 \rangle + \langle u_{33}^2 \rangle)$ . Fits are described in the text.

be very accurate over a wide range of materials (for instance, see Ref. 14). XAFS amplitudes are subject to an overall reduction factor  $S_0^2$ , which was determined by assuming full occupancy of all sites and averaging initial fit amplitudes at all temperatures for each material. The shifts in the threshold energy  $\Delta E_0$  between the data and the fitting standard were obtained in a similar manner.

In analyzing errors from XAFS measurements, it is important to differentiate between the random errors caused by counting statistics, thermal fluctuations, etc., and the absolute, systematic errors caused by the fitting procedure. For much of this paper, we are more concerned with the random errors that occur from one temperature to the next. In these cases, we estimate this error by collecting about three scans at each temperature point for each sample, and fitting each scan individually. These errors are typically quite small, and as such are sometimes not shown in the figures. Where appropriate, we estimate absolute errors by a Monte Carlo method whereby the total error per data point is estimated by assuming the statistical- $\chi^2/\nu = 1$  and that the degrees of freedom  $\nu$  are given by the maximum degrees of freedom from Stern's rule<sup>16</sup> minus the number of fit parameters. Once the total error is obtained, we estimate the error on a fit parameter by finding the point in a fit where the statistical- $\chi^2$  is increased by a factor of one. Generally speaking, absolute errors on nearest-neighbor bond lengths for well-ordered reference crystals have been shown to be  $\sim 0.005 \text{ \AA}$ <sup>14</sup> by comparing to diffraction measurements. Errors in bond length distribution widths ( $\sigma$ ) are around 5% for nearest-neighbors and about 10% for

further neighbors that are relatively well isolated, such as La-La paths in LaB<sub>6</sub>.

### III. RESULTS

#### A NPD data and Rietveld structural refinements

An example of the room temperature NPD data from a backscattering bank is shown in Fig. 3, and the fitting results are summarized in Table I. Anisotropic displacement parameters for the boron site were necessary to obtain high quality fits, as expected from previous studies.<sup>17</sup>

Fits of the displacement parameters to an Einstein model were performed to verify that the displacements are dominated by phonon vibrations and not to positional disorder. Fits to the boron displacements necessarily used the isotropic form of  $\langle u^2 \rangle$ , namely  $(\langle u_{11}^2 \rangle + \langle u_{22}^2 \rangle + \langle u_{33}^2 \rangle)/3$ . The following equation was used for the fit:

$$\langle u_{\text{fit}}^2 \rangle = \langle u_{\text{static}}^2 \rangle + \frac{\hbar^2}{k_B m_A \Theta_E} \left[ \frac{1}{e^{\Theta_E/T} - 1} + \frac{1}{2} \right]. \quad (1)$$

The  $\langle u_{\text{static}}^2 \rangle$  term is a measure of the static or positional disorder in the material, although it can be highly correlated with other parameters in the fits, such as the site occupation. The rest of the equation gives the vibration expected for an atom of mass  $m_A$  with a single vibrational frequency given by the Einstein temperature  $\Theta_E$ . Note that even without any static disorder, the Einstein model predicts a non-zero  $\langle u_{\text{fit}}^2 \rangle$  at zero temperature, as expected for a quantum mechanical harmonic oscillator. In the absence of disorder, the value of this intercept is inversely proportional to  $\Theta_E$ . The data fit this model very well (Fig. 4), with the La site having  $\Theta_E = 140(3)$  K and  $\langle u_{\text{static}}^2 \rangle = 0.00035(6)$  Å<sup>2</sup>, and the B site having  $\Theta_E = 600(25)$  K and  $\langle u_{\text{static}}^2 \rangle = 0.0001(2)$  Å<sup>2</sup>. These measurements of  $\Theta_E$  are consistent with previous studies.<sup>18,19</sup> Moreover  $\langle u_{\text{static}}^2 \rangle$  for the La site was found to be correlated with the La-site occupancy; fits that held the La-site occupancy at unity did not require any  $\langle u_{\text{static}}^2 \rangle$  component. These results attest to the lack of significant positional disorder in this compound.

#### B XAFS data and the local structure

An example of the low temperature XAFS data is shown in  $k$ -space in Fig. 5 and in  $r$ -space in Fig. 6. Fig. 6 shows an example of the fit quality and the fit results are summarized in Table II. The bond displacement parameters are shown in Fig. 7, and the displacement parameters for LaB<sub>6</sub> are also shown in Fig. 4 for comparison to the NPD results.

As can be seen in Table II, the bond lengths measured locally with XAFS are very similar to the average distances between the sites measured with diffraction. The differences in bond lengths are indicative of the absolute error between diffraction and XAFS measurements of  $\approx 0.005$  Å.<sup>14</sup> In other words, the local and average structures are the same for these compounds. When comparing displacement parameters, it is important to remember that in XAFS measurements, the Debye-Waller factor  $\sigma^2$  is the variance in the *bond length* distribution, and therefore includes correlations in the displacements of neighboring atoms. Usually one expects a smaller measurement of  $\sigma^2$  than of  $\langle u^2 \rangle$ , which is what is observed. This will be discussed in more detail below.

In a similar manner as above, we checked the Debye-Waller factors against an Einstein model to determine if any unusual behavior exists in either the vibrational modes or the static displacements. The fitting function is nearly identical to Eq. 1 except that we replace  $\langle u_{\text{static}}^2 \rangle$  with  $\sigma_{\text{static}}^2$  and  $m_A$  with the reduced mass for the atom pair  $\mu_{AB}$ . This model was found to work well for the RE-RE pairs (see Fig. 4); for instance, for La-La pairs the Einstein model gives  $\Theta_E = 130(3)$  K and  $\sigma_{\text{static}}^2 = 0.0000(3)$  Å<sup>2</sup>. However, this model could not describe the temperature dependence of the Debye-Waller factors for the nearest-neighbor RE-B pairs. In essence, the low temperature  $\sigma^2$  expected from zero-point motion in the Einstein model indicates a rather high  $\Theta_E$ , yet the Debye-Waller factors increase much more quickly than such a model would suggest. No amount of *positive*  $\sigma_{\text{static}}^2$  offset can account for this behavior. Given the low value of static displacements for all other measurements up to this point, we assume that the structure is well ordered and try other models of the phonon density of states. Using a Debye form does not help, but if we allow for two Einstein modes, we obtain the fit shown in Fig. 4 for LaB<sub>6</sub>. This fit has 20% of the spectral weight in a mode at 85 K and 80% in a mode at 570 K. A fit that allows for a distribution of modes centered around these two Einstein frequencies gives a very large width for the lower mode of about 50 K.

#### C XAFS of EuB<sub>6</sub> near the ferromagnetic transition

In order to search for structural changes associated with the ferromagnetic transition at 15 K in EuB<sub>6</sub>, we collected data at 3.3, 10, 15, and 20 K. No obvious change occurs in  $\sigma^2$  over this temperature region (Fig. 7). In order to look for very small changes, we elected to fit the data at 10, 15, and 20 K using either the 3.3 K or the 10 K data as a standard rather than using theoretical standard curves, depending on the experimental run in which the data was collected. This method has several advantages when one only cares about changes in a sample from one temperature to the next. For instance, since  $S_0^2$  should be identical for each temperature, the backscattering am-

TABLE I: Final refined structure parameters for the  $\text{La}^{11}\text{B}_6$  sample. Extinction was held at zero in these fits because of a strong correlation with the absorption coefficient.

General fit characteristics:					
Banks included	$\pm 145^\circ, \pm 90^\circ$				
Total data points	16104				
Total measured reflections	264				
# of variables	11 + 20 for background				
$T$ (K)	10 K	100 K	200 K	300 K	
$a_0$ ( $\text{\AA}$ )	4.1527(1)	4.1528(1)	4.1542(1)	4.1561(1)	
La occupancy	0.983(4)	0.987(4)	0.987(4)	0.983(4)	
$x_B$	0.1993(1)	0.1994(1)	0.1994(1)	0.1995(1)	
$\langle u_{\text{iso}}^2 \rangle (\text{La})$ ( $\text{\AA}^2$ )	0.00157(6)	0.0025(2)	0.0042(2)	0.0056(2)	
$\langle u_{11}^2 \rangle (\text{B})$ ( $\text{\AA}^2$ )	0.0027(1)	0.0028(1)	0.0033(1)	0.0035(2)	
$\langle u_{22}^2 \rangle = \langle u_{33}^2 \rangle (\text{B})$ ( $\text{\AA}^2$ )	0.0041(1)	0.0042(1)	0.0047(1)	0.0054(1)	
absorb. coeff.	0.346(2)	0.348(2)	0.363(2)	0.379(3)	
reduced $\chi^2$	3.14	2.04	1.88	1.78	
$Rp$ (%)	3.47	3.92	3.75	3.73	
$wRp$ (%)	4.95	5.57	5.38	5.33	

plitudes can be fixed. Also, using the same material as a standard allows a better determination of the line shapes used in the fits, since systematic errors in the theoretical line shapes exist.<sup>14</sup> In addition, many sources of systematic errors can be removed with this method, such as those that occur from monochromator glitches and bad forms for the pre-edge background and/or  $\mu_0$  functions. This method is still sensitive to drifts in the monochromator calibration from scan to scan, so the value of  $E_0$  remains a fitting parameter. In these fits, we will fix the bond lengths at the experimental standard value, since x-ray diffraction measurements indicate that the lattice parameter does not change within 0.0005  $\text{\AA}$  around the FM transition.<sup>10</sup> These constraints leave a change in  $\sigma^2$  as the only meaningful parameter left in the fits.

These difference fits were broken into three separate regions. The first region is between 2.0 and 3.0  $\text{\AA}$  and corresponds to the Eu-B nearest neighbor scattering. The third region is between 3.5 and 4.3  $\text{\AA}$ , and corresponds mostly to the Eu-Eu scattering, although there is a component from the next neighbor Eu-B scatter near 4.5  $\text{\AA}$ . (Note that the peaks in the XAFS transforms are shifted from the actual pair distances due to the backscattered photoelectron phase shift  $\delta_e(k)$ , as described in Sec. II. This shift is roughly 0.4  $\text{\AA}$  for RE-B pairs and 0.2  $\text{\AA}$  for RE-RE pairs.) The second region is between the first and the third (actually we chose between 3.0 and 3.6  $\text{\AA}$ ) and is meant to look for changes corresponding to the multiple scattering Eu-B-B near 3.9  $\text{\AA}$ . The fit results are shown in Table III and an example of the fit quality is shown in Fig. 8. Fitted  $\Delta E_0$ 's indicate small calibration changes between scans. Fitted  $\Delta\sigma^2$ 's are likely due to systematic errors not removed by this procedure, and should therefore be taken as upper limits for any possible real changes. We consider these upper limit of changes

TABLE II: Fit results for XAFS data at 12 K for the  $\text{La}^{11}\text{B}_6$  sample and at 20 K for the  $\text{EuB}_6$  sample. These fits use  $S_0^2 = 1.02$  for  $\text{LaB}_6$  and 1.00(5) for  $\text{EuB}_6$ , and  $\Delta E_0 = -9.7$  eV for both materials. The RE-B-B multiple scattering peak (equivalent bond length of 3.9  $\text{\AA}$ ) and the RE-B pair at 4.5  $\text{\AA}$  were included in the fits to ensure accurate results for the main single scattering pairs, but their parameters were severely constrained and are not reported here. Errors are estimated from a Monte Carlo method. See Sec. II for details of methods.

bond	$N$	$\sigma^2(\text{\AA}^2)$	$R(\text{\AA})$	$R_{\text{NPD}}(\text{\AA})$
La-B	24	0.0036(3)	3.057(2)	3.0510
La-La	6	0.0011(3)	4.148(4)	4.1527
Eu-B	24	0.0039(4)	3.078(2)	3.0786 <sup>a</sup>
Eu-Eu	6	0.0023(4)	4.182(4)	4.1852 <sup>a</sup>

<sup>a</sup>from Ref. 10

over these temperature ranges to be about  $2.4 \times 10^{-5} \text{\AA}^2$  for the nearest neighbor Eu-B pairs,  $6.2 \times 10^{-5} \text{\AA}^2$  for the Eu-B-B multiple scattering pairs, and  $2.9 \times 10^{-5} \text{\AA}^2$  for the Eu-Eu pairs.

## IV. DISCUSSION

### A General features and overall temperature dependence

The results of the fits to the NPD data indicate that these samples are similar in structure to previously measured samples of  $\text{LaB}_6$ , although the measured room temperature lattice constant of 4.1561(1)  $\text{\AA}$  is somewhat

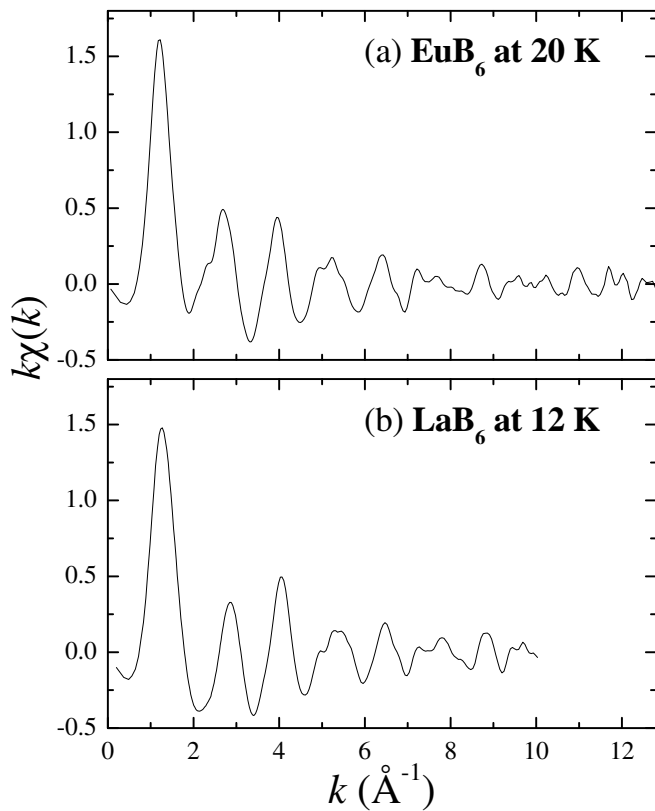


FIG. 5: Representative XAFS data in  $k$ -space for (a)  $\text{EuB}_6$  and (b)  $\text{LaB}_6$ . Data ranges are limited by the proximity of the  $L_{\text{II}}$  edge for each compound.

lower than the canonical value of  $4.1566 \text{ \AA}$ .<sup>20</sup> This difference could indicate some vacancies in the structure, and indeed, our fits are slightly improved by allowing for  $\approx 2\%$  La vacancies. However, a previous study<sup>17</sup> showed that the  $\text{LaB}_6$  lattice constant is relatively insensitive to vacancies. Also, although the fit was improved by including 2% La vacancies, this value was observed to be correlated to both the displacement parameters and the absorption coefficient. Another possibility is that the increased boron mass affects the room temperature lattice constant, such as may occur in  $\text{Sm}^{11}\text{B}_6$  (compare lattice constants in Refs. 21 and 22) and  $\text{Nd}^{11}\text{B}_6$  (Refs. 21 and 23). A third possibility is that the enhanced absorption of the sample cause a lower effective flight path of the diffracted neutrons, causing a reduction in the measured lattice constant. Therefore, we take the measurement of 2% La vacancies and the slightly reduced lattice parameter to be consistent with stoichiometric  $\text{LaB}_6$  for these data. Otherwise, the sample and data quality are good, and the fits are excellent. Similarly, the electronic and magnetic properties of our  $\text{EuB}_6$  sample are consistent with those in previously published studies<sup>10</sup> (Fig. 2). The XAFS fits indicate that the local and average structures are similar, since the La-B, La-La, Eu-

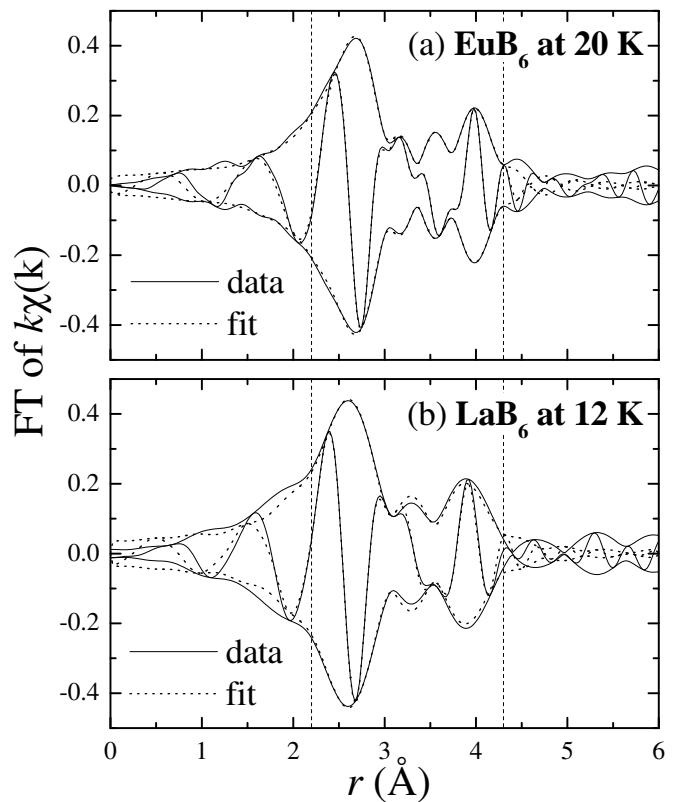


FIG. 6: Representative XAFS data and fits in  $r$ -space for (a)  $\text{EuB}_6$  and (b)  $\text{LaB}_6$ . Fit ranges are shown. Transform ranges are (a)  $2.5\text{-}12.3 \text{ \AA}^{-1}$  and (b)  $2.5\text{-}10.3 \text{ \AA}^{-1}$ , each Gaussian narrowed by  $0.3 \text{ \AA}^{-1}$ .

B and Eu-Eu bond lengths are consistent with this (for  $\text{La}^{11}\text{B}_6$ ) and previous diffraction studies (for both  $\text{LaB}_6$  and  $\text{EuB}_6$ ).<sup>10,18,19</sup>

We do, however, measure previously unreported behavior for the site ( $\langle u^2 \rangle$ ) and pair ( $\sigma^2$ ) displacement parameters for RE-B pairs as a function of temperature, namely that although the site displacement parameters for  $\text{LaB}_6$  fit an Einstein model well, the displacements as measured by XAFS for both  $\text{LaB}_6$  and  $\text{EuB}_6$  require at least two Einstein frequencies. This unusual situation can be understood by considering the relationship between the site displacement parameters from NPD (the  $\langle u^2 \rangle$ 's) and the bond displacement parameters from XAFS (the  $\sigma^2$ 's). If one considers the  $u$  parameter as an instantaneous displacement from the mean position of atom  $A$ , then the average  $A - B$  bond length distribution width  $\sigma^2$  is given by the time averages of:

$$\begin{aligned} \sigma^2 &= \langle (u_A - u_B)^2 \rangle \\ &= \langle u_A^2 \rangle + \langle u_B^2 \rangle - 2 \langle u_A u_B \rangle \\ &= \langle u_A^2 \rangle + \langle u_B^2 \rangle - 2 \sqrt{\langle u_A^2 \rangle \langle u_B^2 \rangle} \phi \quad (2) \end{aligned}$$

where the  $\phi$  parameter is a measure of the correlation be-

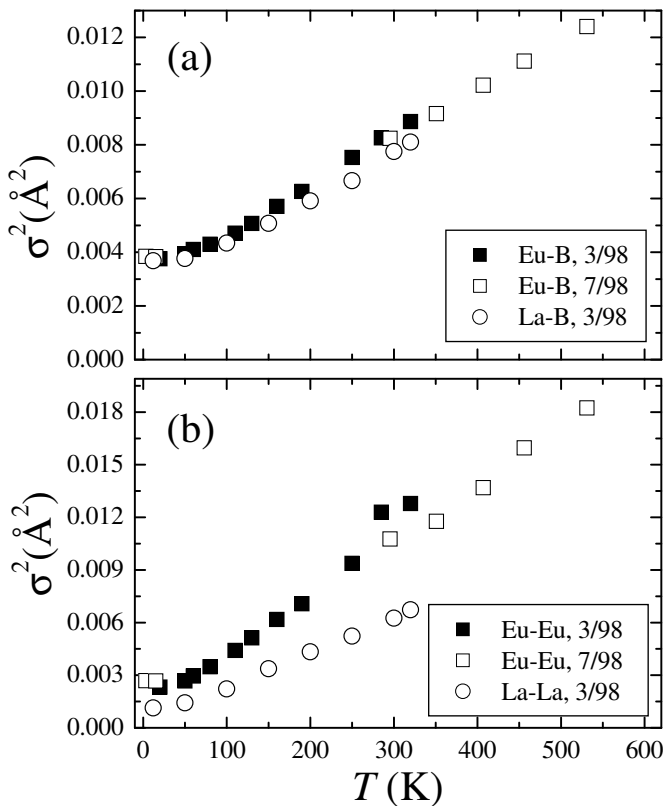


FIG. 7: Debye-Waller factors for single scattering paths in XAFS fits from various experimental runs. LaB<sub>6</sub> data from Fig. 4 are repeated here for comparison. Estimated random errors are smaller than the plot symbols. Absolute errors are about 10% for RE-B pairs and 20% for RE-RE pairs.

tween the displacements of atoms  $A$  and  $B$ ; for uncorrelated displacements,  $\phi=0$ , if the displacements are always in the same direction (as in an acoustic phonon)  $\phi=1$ , and if the displacements are always in opposite directions (as in a ferroelectric distortion, or an optical phonon)  $\phi=-1$ . Although there are still few measurements of this sort (one needs both local and average structure data), it appears that for nearest neighbors in systems where the bonding is not predominantly metallic,  $\phi$  is generally close to one. For instance, for the Hg-O(2) pairs in HgBa<sub>2</sub>CuO<sub>4</sub>,  $\phi \simeq 0.9$ ,<sup>24</sup> and Cu-O(4) in YBa<sub>2</sub>Cu<sub>3</sub>O<sub>7</sub>,  $\phi \simeq 0.85$ .<sup>25</sup> For the second neighbor metal atoms in these systems (such as the Cu-Ba pairs in YBa<sub>2</sub>Cu<sub>3</sub>O<sub>7</sub>)  $\phi$  is generally near 0.5. Pair-distribution function analysis of diffraction data can yield  $\phi$  using a single data set. In InAs, nearest-neighbor In-As pairs have  $\phi \approx 0.8$ .<sup>26</sup> For further comparison, the Ni-Ni nearest neighbors in Ni metal have a relatively low  $\phi$  of about 0.3.<sup>26</sup> In all these cases, as the bond length increases,  $\phi$  tends to get smaller.

Since we collected NPD and XAFS data on similar samples of La<sup>11</sup>B<sub>6</sub>, we can calculate  $\phi$  for the La-B and

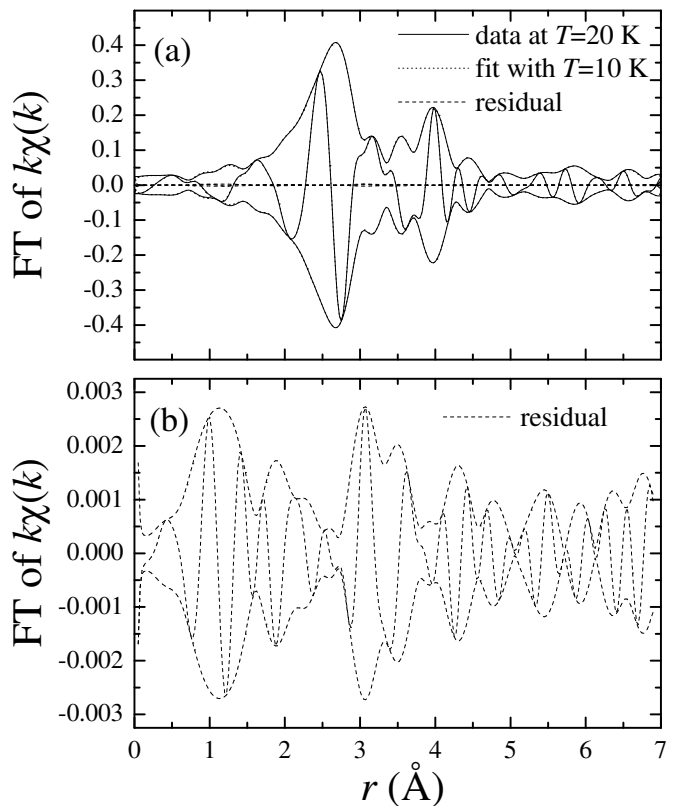


FIG. 8: (a) Representative experiment-standard fit for EuB<sub>6</sub>. Fit is almost perfect, and hence difficult to see. Residual is also shown, and repeated with a different scale in panel (b) for clarity.

La-La pairs, and these results are shown in Fig. 9. The magnitude of  $\phi$  for the La-La pairs is as expected from the copper oxides,<sup>24,25</sup> except that we measure a decrease in  $\phi$  with temperature. This decrease may be an artifact of the absorption coefficient in the Rietveld refinement; when the La occupancy is held at unity, the fitted  $\langle u^2 \rangle$ 's give a nearly constant  $\phi$  of about 0.55. The La-B pairs, on the other hand, are nearly uncorrelated in their displacements, giving the unusual situation where the displacements of the relatively short La-B pairs at 3.05  $\text{\AA}$  are less correlated than the La-La pairs at 4.15  $\text{\AA}$ . Since the NPD data clearly indicate no positional disorder, these measurements are direct structural evidence that the La and B sublattices are nearly uncoupled in their vibrations. This result, in turn, suggests that the dominant frequency distribution in the La-B pair vibrations is bimodal, and indeed, the  $\sigma^2$  vs.  $T$  data fit such a distribution well. Since the EuB<sub>6</sub> XAFS data is so similar to the LaB<sub>6</sub> data, this result can be applied to EuB<sub>6</sub>, as well. Comparisons to optical reflectivity data are possible when one considers that the Einstein fits to the XAFS data are to be taken as a weighted average of all other modes present and therefore cannot exactly correspond to a given mode. With this caveat in mind,

TABLE III: Fit results for  $\text{EuB}_6$  XAFS data using low temperature data on  $\text{EuB}_6$  as a fitting standard rather than theoretical standards. Results are therefore changes in the listed parameters between the temperature of the standard and the temperature of the data. Errors in parentheses are obtained by a Monte Carlo method. Changes in  $E_0$  indicate small shifts in the monochromator calibration. Non-zero measurements of  $\Delta\sigma^2$  are likely due to systematic errors in data reduction and collection and therefore these measurements should be considered as upper limits on any such possible changes.

Temperature pair	$\Delta E_0$ (eV)	$\Delta\sigma^2$ ( $\text{\AA}^2$ )
<i>Eu-B range: 2.0-3.0 \AA</i>		
20 K - 10 K	0.31(1)	$4.0(12) \times 10^{-6}$
15 K - 10 K	0.20(1)	$-1.8(3) \times 10^{-5}$
15 K - 3.3 K	0.02(1)	$-2.4(4) \times 10^{-5}$
<i>Eu-B-B range: 3.0-3.6 \AA</i>		
20 K - 10 K	0.24(3)	$6.2(16) \times 10^{-5}$
15 K - 10 K	0.16(2)	$1.1(5) \times 10^{-5}$
15 K - 3.3 K	0.00(2)	$-4.5(9) \times 10^{-5}$
<i>Eu-Eu range: 3.5-4.3 \AA</i>		
20 K - 10 K	0.32(2)	$2.9(3) \times 10^{-5}$
15 K - 10 K	0.20(1)	$-9.6(1.2) \times 10^{-6}$
15 K - 3.3 K	0.02(1)	$-8.4(1.1) \times 10^{-6}$

these results are in approximate agreement with optical reflectivity data that shows a B-B mode in  $\text{EuB}_6$  at  $850 \text{ cm}^{-1}$  (1223 K) and a Eu-B mode at  $145 \text{ cm}^{-1}$  (209 K)<sup>7</sup> if the B-B mode dominates the Eu-B mode.

### B Lattice involvement in $\text{EuB}_6$ magnetoresistance transition

Now that we have established the “canonical” hexaboride structural and vibrational behavior by looking at  $\text{LaB}_6$ , we turn to the question of whether there is a lattice involvement in the magnetoresistance transition of  $\text{EuB}_6$ .

Previous average structural studies of the lattice parameters and our measurements of the Eu-B and Eu-Eu local displacement parameters (Fig. 7) show no obvious change near  $T_C$ . In order to place limits on this lack of change, we used the low temperature data to fit the higher temperature data in the vicinity of the FM transition. The results are summarized in Table III. We expect some change over this temperature range due to thermal broadening of about  $1 \times 10^{-5} \text{ \AA}^2$  and  $2 \times 10^{-5} \text{ \AA}^2$  for Eu-B and Eu-Eu, respectively, so the maximum additional change due to any possible polaronic effects from these measurements are  $\Delta\sigma_P^2(\text{Eu-B}) = 1.5 \times 10^{-5} \text{ \AA}^2$  and  $\Delta\sigma_P^2(\text{Eu-Eu}) = 1 \times 10^{-5} \text{ \AA}^2$ . For comparison, we measure  $\Delta\sigma_P^2(\text{Mn-O}) = 3.5 \times 10^{-3} \text{ \AA}^2$  in the

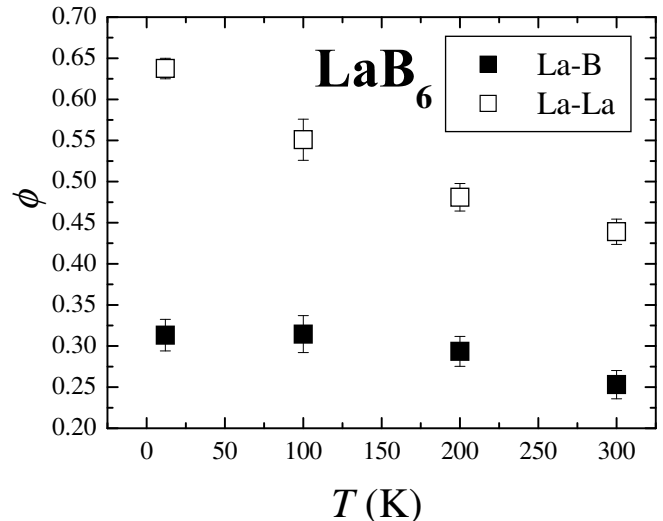


FIG. 9: Correlation parameter for displacements between La and B nearest neighbors and La and La neighbors. Error bars are based on reproducibility from scan to scan. Systematic errors are estimated to be as large as 0.1, so the apparent decrease in  $\phi$  may be an experimental artifact.

CMR perovskite  $\text{La}_{2/3}\text{Ca}_{1/3}\text{MnO}_3$ , which is two orders of magnitude larger.<sup>11</sup>

This result clearly indicates a smaller degree of lattice involvement in  $\text{EuB}_6$  compared to the CMR perovskites. To quantify this involvement, we need to know the number of Eu atoms that are involved in the magnetic polarons. The analysis of the Raman scattering<sup>8</sup> suggests that only 3% of the Eu atoms are so involved. Under these circumstances, our measurement translates to an upper limit of roughly  $5 \times 10^{-4} \text{ \AA}^2$ , or  $0.02 \text{ \AA}$  for the distortion around each Eu atom in the polaron. In the case of the CMR perovskite oxides, the distortion is associated with a valence fluctuation between the  $\text{Mn}^{3+}$  and  $\text{Mn}^{4+}$  valence states. For  $\text{EuB}_6$  we can use the difference in lattice parameter between divalent and trivalent rare-earth hexaborides<sup>1</sup> to estimate that the distortion resulting from a valence fluctuation to  $\text{Eu}^{3+}$  should be about  $0.07 \text{ \AA}$ . Our upper limit is well below this value, which strengthens the case for the dissimilarity between the behavior of  $\text{EuB}_6$  and the CMR perovskites. We should add that the estimate that only 3% of the Eu atoms are involved in the polarons is based on analogy to spin-flip Raman scattering in dilute magnetic semiconductors such as  $\text{Cd}_{1-x}\text{Mn}_x\text{Te}$ ;<sup>27</sup> it is by no means clear that the theory can be simply extended to the case of a full lattice of magnetic ions. Since the density and size of magnetic polarons are not well established for  $\text{EuB}_6$ , there may be far more than 3% Eu atoms involved in the polarons.<sup>28</sup> In fact,  $\sim 15\%$  of the volume is ferromagnetically aligned at the 15.5 K transition.<sup>5</sup> If this



volume fraction is more indicative of the number of Eu atoms involved in the magnetic polaron, then our results would imply an even smaller distortion ( $\sim 0.004 \text{ \AA}$ ) per Eu atom.

The difference in lattice polaron size between  $\text{EuB}_6$  and the CMR perovskites underscores the essential difference in the mechanism for the large magnetoresistance in these materials. The CMR perovskites have a high electrical resistance in their normal (above  $T_C$ ) state because conduction is strongly impeded by charges trapped by local lattice distortions. These lattice polarons are large enough and prevalent enough that other conducting pathways are excluded; that is, the system has not reached the percolation limit. When the system becomes magnetic, spin alignment encourages the charge to flow, essentially removing the lattice polarons and putting the system beyond the percolation limit. It is very difficult to imagine how this basic picture can apply to  $\text{EuB}_6$  given that the average distortion around a Eu site is more than an order of magnitude smaller than in the perovskites. Therefore, we conclude that any possible dynamic lattice interaction is playing a very small role in the  $\text{EuB}_6$  MR, and is probably incidental. Although in  $\text{EuB}_6$  lattice polarons aren't contributing to the magnetoresistance, we emphasize that these measurements are not sensitive to magnetic polarons.

## V. CONCLUSION

In conclusion, we have measured the local and average structure of  $\text{LaB}_6$  and compared these data to local structure data on  $\text{EuB}_6$ . These lattices have similar static and thermal properties: they are crystallographically well ordered with no measurable positional disorder, and the La/Eu sublattice is vibrationally decoupled from the B sublattice. Furthermore, we have placed stringent limits on the degree of change in the local structure around Eu in the vicinity of the ferromagnetic/magnetoresistive transition near 15 K. This result serves to underscore the fundamental difference between the CMR perovskites and  $\text{EuB}_6$ : although magnetic polarons (i.e. electrons coupled to short-range magnetic order) exist in both systems, the lattice involvement in the perovskites is orders of magnitude more pronounced, suggesting that any possible dynamical lattice polarons in  $\text{EuB}_6$  play an incidental role.

## ACKNOWLEDGMENTS

The authors thank J. D. Thompson for useful conversations. We also thank F. Bridges, M. Anderson, D. Cao, J. Richardson and C. Murphy for assistance in collecting the data. This work was partially supported by the Office of Basic Energy Sciences (OBES), Chemical Sciences Division of the U. S. Department of Energy (DOE),

Contract no. DE-AC03-76SF00098, and by the National Science Foundation, grant no. 9971348. Work at Los Alamos National Laboratory was conducted under the auspices of the DOE. XAFS data were collected at the Stanford Synchrotron Radiation Laboratory, which is operated by the DOE/OBES. Neutron data were collected at the Intense Pulsed Neutron Source at Argonne National Laboratory, which is funded by the DOE under Contract W-31-109-ENG-38.

## REFERENCES

- <sup>†</sup> Electronic address: [chbooth@lbl.gov](mailto:chbooth@lbl.gov)
- <sup>1</sup> J. Etourneau and P. Hagenmuller, *Phil. Mag.* **B 52**, 589 (1985).
  - <sup>2</sup> S. Massidda, A. Continenza, T. M. de Pascale, and R. Monnier, *Z. Phys. B* **102**, 83 (1997).
  - <sup>3</sup> Z. Fisk, D. C. Johnston, B. Cornut, S. von Molnar, S. Oseroff, and E. Calvo, *J. Appl. Phys.* **50**, 1911 (1979).
  - <sup>4</sup> M. C. Aronson, J. L. Sarrao, Z. Fisk, M. Whitton, and B. L. Brandt, *Phys. Rev. B* **59**, 4720 (1999).
  - <sup>5</sup> S. Süllow, I. Prasad, M. C. Aronson, S. Bogdanovich, J. L. Sarrao, and Z. Fisk, *Phys. Rev. B* **62**, 11626 (2000).
  - <sup>6</sup> A. P. Ramirez, *J. Phys.: Condens. Matter* **9**, 8171 (1997).
  - <sup>7</sup> L. Degiorgi, E. Felder, H. R. Ott, J. L. Sarrao, and Z. Fisk, *Phys. Rev. Lett.* **79**, 5134 (1997).
  - <sup>8</sup> P. Nyhus, S. Yoon, M. Kauffman, S. L. Cooper, Z. Fisk, and J. Sarrao, *Phys. Rev. B* **56**, 2717 (1997).
  - <sup>9</sup> W. Opechowski and R. Guccione, *Magnetism* (Academic Press, New York, 1965), vol. IIa, p. 105.
  - <sup>10</sup> S. Süllow, I. Prasad, M. C. Aronson, J. L. Sarrao, Z. Fisk, D. Hristova, A. H. Lacerda, M. F. Hundley, A. Vigliante, and D. Gibbs, *Phys. Rev. B* **57**, 5860 (1998).
  - <sup>11</sup> C. H. Booth, F. Bridges, G. H. Kwei, J. M. Lawrence, A. L. Cornelius, and J. J. Neumeier, *Phys. Rev. B* **57**, 10440 (1998).
  - <sup>12</sup> A. C. Larson and R. B. Von Dreele, *Los Alamos National Laboratory Report No. LAUR 86-748* (2000).
  - <sup>13</sup> T. M. Hayes and J. B. Boyce, in *Solid State Physics*, edited by H. Ehrenreich, F. Seitz, and D. Turnbull (Academic, New York, 1982), vol. 37, p. 173.
  - <sup>14</sup> G. G. Li, F. Bridges, and C. H. Booth, *Phys. Rev. B* **52**, 6332 (1995).
  - <sup>15</sup> S. I. Zabinsky, J. J. Rehr, A. Ankudinov, R. C. Albers, and M. J. Eller, *Phys. Rev. B* **52**, 2995 (1995).
  - <sup>16</sup> E. A. Stern, *Phys. Rev. B* **48**, 9825 (1993).
  - <sup>17</sup> G. Koren and E. Polturak, *J. Less-Common Met.* **117**, 73 (1986).
  - <sup>18</sup> D. Yu. Chernyshev, M. M. Korsukova, A. L. Malyshev, V. N. Gurin, V. A. Trunov, V. V. Chernyshev, and L. A. Aslanov, *Phys. Solid State* **36**, 585 (1994).
  - <sup>19</sup> V. A. Trunov, A. L. Malyshev, D. Yu. Chernyshev,

- M. M. Korsukova, and V. N. Gurin, *Phys. Solid State* **36**, 1465 (1994).
- <sup>20</sup> R. W. G. Wyckoff, *Crystal Structures*, vol. 2 (Interscience Publishers, New York, 1964), 2nd ed.
- <sup>21</sup> V. A. Trunov, A. L. Malyshev, D. Yu. Chernyshev, M. M. Korsukova, V. N. Gurin, L. A. Aslanov, and V. V. Chernyshev, *J. Phys.: Condens. Matter* **5**, 2479 (1993).
- <sup>22</sup> A. A. Eliseev, V. A. Efremov, G. M. Kuz'micheva, E. S. Konovalova, V. I. Lazorenko, Yu. B. Paderno, and S. Yu. Khlyustova, *Sov. Phys. Crystallogr.* **31**, 476 (1986).
- <sup>23</sup> M. K. Blomberg, M. J. Merisalo, M. M. Korsukova, and V. N. Gurin, *J. of Alloys and Compounds* **217**, 123 (1995).
- <sup>24</sup> C. H. Booth, F. Bridges, E. D. Bauer, G. G. Li, J. B. Boyce, T. Claeson, C. H. Chu, and Q. Xiong, *Phys. Rev. B* **52**, R15745 (1995).
- <sup>25</sup> C. H. Booth, F. Bridges, J. Boyce, T. Claeson, B. M. Lairson, R. Liang, and D. A. Bonn, *Phys. Rev. B* **54**, 9542 (1996).
- <sup>26</sup> I.-K. Jeong, T. Proffen, F. Mohiuddin-Jacobs, and S. J. L. Billinge, *J. Phys. Chem. A* **103**, 921 (1999).
- <sup>27</sup> D. L. Peterson, D. U. Bartholomew, E. Debska, A. K. Ramdas, and S. Rodriguez, *Phys. Rev. B* **32**, 323 (1985).
- <sup>28</sup> C. S. Snow, S. L. Cooper, D. P. Young, Z. Fisk, A. Comment, and J. Ansermaet, cond-mat/0011527.